PHYSICAL REVIEW D **93,** 055035 (2016)

Interference effect on a heavy Higgs resonance signal in the $\gamma\gamma$ and ZZ channels

Jeonghyeon Song,[1,*] Yeo Woong Yoon,[1,2,†] and Sunghoon Jung[2,3,‡]

[1]*School of Physics, KonKuk University, Seoul 143-701, Korea*
[2]*School of Physics, Korea Institute for Advanced Study, Seoul 130-722, Korea*
[3]*SLAC National Accelerator Laboratory, Menlo Park, California 94025, USA*

(Received 20 January 2016; published 24 March 2016)

The resonance-continuum interference is usually neglected when the width of a resonance is small compared to the resonance mass. We reexamine this standard by studying the interference effects in high-resolution decay channels, $\gamma\gamma$ and ZZ, of the heavy Higgs boson H in nearly aligned two-Higgs-doublet models. For the H with a sub-percent width-to-mass ratio, we find that, in the parameter space where the LHC 14 TeV ZZ resonance search can be sensitive, the interference effects can modify the ZZ signal rate by $\mathcal{O}(10)\%$ and the exclusion reach by $\mathcal{O}(10)$ GeV. In other parameter space where the ZZ or $\gamma\gamma$ signal rate is smaller, the LHC 14 TeV reach is absent, but a resonance shape can be much more dramatically changed. In particular, the $\gamma\gamma$ signal rate can change by $\mathcal{O}(100)\%$. Relevant to such parameter space, we suggest variables that can characterize a general resonance shape. We also illustrate the relevance of the width on the interference by adding nonstandard decay modes of the heavy Higgs boson.

DOI: 10.1103/PhysRevD.93.055035

I. INTRODUCTION

Needless to say, the 125 GeV Standard Model (SM) Higgs boson discovery at the LHC run I [1] is a big step toward the understanding of the electroweak symmetry breaking. But the observed mass of 125 GeV requires a satisfactory explanation for the huge hierarchy between the weak scale and the Planck scale. Most candidate explanations, such as supersymmetry and composite Higgs models, predict a set of new particles at around the electroweak scale. The absence of any such discovery at the LHC run I motivates us not only to reponder naturalness criteria but also to revisit collider search strategies.

The 13 TeV LHC run II, which started taking data a few months ago, may indeed need a careful study of resonance searches. Unlike usually assumed, a particle somewhat heavier than the electroweak scale may not show up as a Breit-Wigner (BW) resonance peak at the LHC experiments. The resonance-continuum interference can induce observable impacts on the production rate and the invariant mass distribution (resonance shape). It is generally because (a) a heavier particle can be broader (more decay channels with less phase-space suppression and possible Goldstone enhancements), and (b) the production and decay amplitudes can involve complex phases that arise from SM particles running in loops below the threshold. Various studies have shown that the interference for such cases is not usually negligible [2–25].

Most resonance searches at collider experiments model a resonance as a BW peak and estimate the signal rate by the narrow width approximation (NWA). This is justified if the width-to-mass ratio Γ/M is small enough (see e.g., Ref. [26]) and the resonance width is smaller than the experimental resolution. Thus, LHC searches assume 1% Γ/M in the $\gamma\gamma$ channel [27,28] and 0.5% in the ZZ channel [29,30], which imply that the width of a few hundred GeV resonance is similar or smaller than the experimental bin size. But for even a slightly broader resonance, perhaps with some complex phases in its production and decay amplitudes, such an approximation may not be guaranteed. In this paper, we reexamine such an approximation using the two-Higgs-doublet models (2HDM).

A notable example that reveals the dramatic interference effect is the decay of heavy Higgs bosons H and A into the $t\bar{t}$ at hadron colliders [3]. Most strikingly, it was shown that a pure resonance dip is produced in a large part of parameter space [4]. In other parameter space, a general mixture of the real- and the imaginary-part interferences produces a mixture of a peak and a dip in the $m_{t\bar{t}}$ distribution [4,31,32]. Unfortunately, it is difficult to resolve such rich structure of the $t\bar{t}$ resonance shape [31] because the experimental $m_{t\bar{t}}$ resolution $\sim$100 GeV [33,34] is bigger than the typical width of the heavy Higgs bosons in the aligned 2HDM. Although a pure dip can perhaps be well searched using the available techniques optimized for a BW peak [4], it is produced only in some part of the parameter space.

The interference also exists in the high-resolution decay channels, $\gamma\gamma$ and ZZ. The interferences of the SM-like heavy Higgs boson at hadron colliders, $gg \to H \to ZZ, \gamma\gamma$,

*jeonghyeon.song@gmail.com
†ywyoon@kias.re.kr
‡shjung@slac.stanford.edu

have been calculated in past decades [5,6,10,12–16,21]; but they are found to be insignificant producing mostly a BW peak. The main difference between the $t\bar{t}$ and $ZZ, \gamma\gamma$ channels is the relative size of the continuum and the resonance processes [4]. The $t\bar{t}$ experiences a significant interference because the tree-level continuum, B, and the one-loop resonance, S, can produce a loop-factor enhanced interference $\sqrt{SB}/S \sim \sqrt{B/S}$ relative to the resonance squared. While large interference effects might be expected in $gg \to \gamma\gamma$ since the continuum is produced by a one-loop process and the resonance process occurs via two-loops, small interference effects are expected in $gg \to ZZ$ since both continuum and resonance processes are one-loop order. Meanwhile, the off-shell interference of the SM Higgs, which is beyond the scope of this paper, with the continuum ZZ at an invariant mass much bigger than 125 GeV was found to be sensitive to the Higgs width [12,35,36].

Nonetheless, the interference in the ZZ and $\gamma\gamma$ can be more exciting for the 2HDM heavy Higgs bosons. The expectation is again based on a general estimation of the relative interference [4]. In the nearly aligned 2HDM, as is preferred by SM Higgs precision measurements ($|c_{\beta-\alpha}| \lesssim 0.1$–$0.4$ depending on models), the resonance process is suppressed by the small $c_{\beta-\alpha}$ and complex phases can be different in the $\gamma\gamma$ channel as the W boson loop is suppressed. As a result, the interference can be relatively enhanced and the resonance shape can be nontrivially modified. Thus, we study the interference in the ZZ and $\gamma\gamma$ channels in this nearly aligned 2HDM. This setup is not only motivated by Higgs precision measurements, but can illustrate the resonance-continuum interference of a relatively narrow resonance.

The paper is organized as follows. In Sec. II, we review the 2HDM and our formalism of the interference effect on the invariant mass distribution. In addition, we suggest a few variables that can characterize a resonance shape containing a peak and a dip. We then present the results for the $\gamma\gamma$ channel in Sec. III and the ZZ channel in Sec. IV. We also consider the case of a somewhat broader heavy Higgs boson in Sec. V, in which we add nonstandard decay modes. Section VI contains our conclusions.

II. BRIEF REVIEW OF THE 2HDM AND THE INTERFERENCE EFFECTS

A. H in the 2HDM

We consider a 2HDM [37] with CP invariance and softly broken Z_2 symmetry, which introduces two complex Higgs doublet scalar fields, Φ_1 and Φ_2, where

$$\Phi_j \equiv \begin{pmatrix} \phi_j^+ \\ \frac{1}{\sqrt{2}}(v_j + \rho_j^0 + i\eta_j^0) \end{pmatrix}, \tag{1}$$

with $v_1 = v\cos\beta$, $v_2 = v\sin\beta$, and $v = 246$ GeV. The electroweak symmetry breaking is generated by nonzero vacuum expectation value v of a linear combination $H_1 = \cos\beta\Phi_1 + \sin\beta\Phi_2$. Its orthogonal combination $H_2 = -\sin\beta\Phi_1 + \cos\beta\Phi_2$ acquires zero vacuum expectation value. In what follows, we take $s_x = \sin x$, $c_x = \cos x$, and $t_x = \tan x$ for notational simplicity. There are five physical Higgs boson degrees of freedom, the light CP-even scalar $h(= -s_\alpha\rho_1^0 + c_\alpha\rho_2^0)$, the heavy CP-even scalar $H(= c_\alpha\rho_1^0 + s_\alpha\rho_2^0)$, the CP-odd pseudoscalar $A(= -s_\beta\eta_1^0 + c_\beta\eta_2^0)$, and two charged Higgs bosons $H^\pm(= -s_\beta\phi_1^\pm + c_\beta\phi_2^\pm)$, where α is the mixing angle between CP-even Higgses. The SM Higgs field is the CP-even neutral state of H_1:

$$H^{\rm SM} = s_{\beta-\alpha}h + c_{\beta-\alpha}H. \tag{2}$$

Note that if $s_{\beta-\alpha} = 1$, h has the same couplings as the SM Higgs boson, which is preferred by the SM Higgs precision measurement with LHC8 data [38]. This is called the alignment limit [39].

We consider the case where the observed 125 GeV state $H^{\rm SM}$ is the lighter CP-even state h although another interesting possibility of $H^{\rm SM} = H$ is still compatible with the current LHC Higgs data [40–46]. In addition, we assume $s_{\beta-\alpha} > 0$.[1] Focused on $\gamma\gamma$ and ZZ decay modes, we study the gluon fusion production of H in the two-dimensional parameter space of M_H and t_β with the given $c_{\beta-\alpha}$. Another model parameter, the soft Z_2 symmetry breaking term m_{12}^2, is tuned to suppress H-h-h triple coupling λ_{Hhh}, where

$$\lambda_{Hhh} = \frac{c_{\beta-\alpha}}{vs_{2\beta}}\left[\left(\frac{6s_{2\alpha}}{s_{2\beta}} - 2\right)m_{12}^2 - s_{2\alpha}(M_H^2 + 2m_h^2)\right]. \tag{3}$$

The H-V-V ($V = W^\pm, Z$) coupling normalized by the SM value is $c_{\beta-\alpha}$. In order to have $H \to ZZ$, therefore, we need some deviation from the alignment limit. We will therefore consider "nearly aligned" 2HDM in the remainder of this paper.

Yukawa couplings, which play an important role in Higgs phenomenology, are different among the types of 2HDM. In this study, we consider type I and type II where the normalized Yukawa couplings by the SM values, $\hat{y}^H_{t,b,\tau}$, in terms of $c_{\beta-\alpha}$ and $s_{\beta-\alpha}$ are

	$c_{\beta-\alpha} - \frac{s_{\beta-\alpha}}{t_\beta}$	$c_{\beta-\alpha} + t_\beta s_{\beta-\alpha}$
Type I	$\hat{y}^H_t, \hat{y}^H_b, \hat{y}^H_\tau$	
TypeII	$\hat{y}^H_t$	$\hat{y}^H_b, \hat{y}^H_\tau$

(4)

[1]Note that the wrong sign case in the 2HDM is shown to be still allowed by the current LHC Higgs signal strength measurements, though less probable [46].

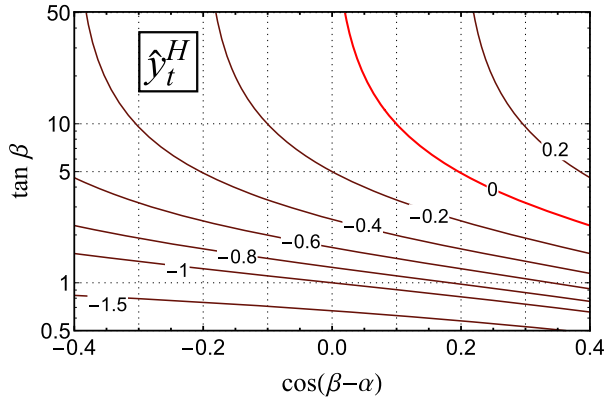

FIG. 1. The top quark Yukawa coupling $\hat{y}_t^H$ normalized by the SM one is shown in the $(c_{\beta-\alpha}, t_\beta)$ plane for $s_{\beta-\alpha} > 0$. We mark the top-phobic $\hat{y}_t^H = 0$ contour with brighter red.

Note that both type I and type II have the same top quark Yukawa coupling.

We find that there exists a special parameter choice for $\hat{y}_t^H = 0$, called the top-phobic H. To be more specific, we present the value of $\hat{y}_t^H$ in the parameter space of $(c_{\beta-\alpha}, t_\beta)$ in Fig. 1. As the red line indicates, a specific *nonzero positive* $c_{\beta-\alpha}$ for a given t_β leads to vanishing $\hat{y}_t^H$, which happens, for example, when $t_\beta = 10$ for $c_{\beta-\alpha} = 0.1$ or $t_\beta = 2.3$ for $c_{\beta-\alpha} = 0.4$. Near the top-phobic line the signal rate is severely suppressed especially for type I.

B. General formalism for interference

We consider the interference between the continuum background and the resonance process of a particle with mass M and total decay width Γ in a $2 \to 2$ scattering process. When we write the helicity amplitudes for the continuum background ($\mathcal{M}_{\rm cont}$) and the resonance ($\mathcal{M}_{\rm res}$) as

$$\mathcal{M}_{\rm cont} = \mathcal{A}_{\rm cont} e^{i\phi_{\rm cont}},$$
$$\mathcal{M}_{\rm res} = \frac{M^2}{\hat{s} - M^2 + iM\Gamma} \mathcal{A}_{\rm res} e^{i\phi_{\rm res}}, \tag{5}$$

the total partonic cross section becomes

$$\hat{\sigma}_{\rm cont} + \hat{\sigma}_{\rm sig} = \hat{\sigma}_{\rm cont} + \hat{\sigma}_{\rm res} \frac{M^4}{(\hat{s} - M^2)^2 + M^4 w^2} \times \left[1 + \frac{2w}{R} \sin\phi + \frac{2(\hat{s} - M^2)}{M^2} \frac{\cos\phi}{R}\right]$$
$$\equiv \hat{\sigma}_{\rm cont} + \hat{\sigma}_{\rm res}[f_{\rm BW}(m_{\rm inv}) + f_{\rm Im}(m_{\rm inv}) + f_{\rm Re}(m_{\rm inv})], \tag{6}$$

where $m_{\rm inv} = \sqrt{\hat{s}}$. Note that $f_{\rm BW}, f_{\rm Im}, f_{\rm Re}$ take the terms in square brackets one by one. $\hat{\sigma}_{\rm cont}$, $\hat{\sigma}_{\rm res}$, R, and the interference phase ϕ are

$$\hat{\sigma}_{\rm cont,res} = \frac{1}{32\pi\hat{s}} \int dz \sum \mathcal{A}^2_{\rm cont,res},$$
$$\hat{\sigma}_{\rm int} e^{i\phi} = \frac{1}{32\pi\hat{s}} \int dz \sum \mathcal{A}_{\rm cont} \mathcal{A}_{\rm res} e^{i(\phi_{\rm res} - \phi_{\rm cont})},$$
$$R = \frac{\hat{\sigma}_{\rm res}}{\hat{\sigma}_{\rm int}}, \qquad w \equiv \frac{\Gamma}{M}, \tag{7}$$

where $z = \cos\theta^*$ while θ^* is the scattering angle in the c.m. frame. The summation is over helicity and color indices. R, w, and ϕ are the key parameters which determine the pattern of interference effect. A more intuitive form for R and ϕ can be obtained if we assume that one helicity amplitude is dominant:

$$R \simeq \frac{\mathcal{A}_{\rm res}}{\mathcal{A}_{\rm cont}}, \qquad \phi \simeq \phi_{\rm res} - \phi_{\rm cont}. \tag{8}$$

As can be understood from Eq. (6) and will be discussed more, w/R indicates the strength of interference effect and ϕ determines whether it is imaginary-part interference ($c_\phi = 0$) or real-part interference ($s_\phi = 0$), or between the two.

Most of the new particles of our interest have narrow width ($w \ll 1$), which confines the signal events in the resonance region of the invariant mass distribution. It is a good approximation to ignore the $m_{\rm inv}$ dependence of R and ϕ. Then $m_{\rm inv}$ dependence of $\hat{\sigma}_{\rm sig}$ is explicitly shown in Eq. (6) as a simple function of $\hat{s}$ ($= m^2_{\rm inv}$). Apparently, $f_{\rm Re}(m_{\rm inv})$ is an odd function at $m_{\rm inv} = M$, which yields a dip-peak or peak-dip structure. On the contrary $f_{\rm BW}(m_{\rm inv})$ and $f_{\rm Im}(m_{\rm inv})$ are even functions. The sensitivity to $f_{\rm Re}(m_{\rm inv})$ and $f_{\rm Im}(m_{\rm inv})$ crucially depends on the bin size of the invariant mass distribution. If the bin is large such that a dip-peak structure is included in one bin, we should integrate over $m_{\rm inv}$, which eliminates the real-part interference. If the bin is narrow enough, a more dynamic structure of $f_{\rm Re}$ can be probed. We consider these two cases and suggest new observation factors for each case.

(i) *Large bin.*—In this case, we integrate $\hat{\sigma}_{\rm sig}$ over $m_{\rm inv}$, under which the even functions survive but the odd function $f_{\rm Re}(m_{\rm inv})$ is washed out at leading order.[2] The survived imaginary part interference results in a multiplicative factor, $(1 + 2w \sin\phi/R)$, to the NWA rate $\sigma \cdot {\rm Br}$. Therefore, the total signal rate can significantly differ from what was obtained from the NWA due to the imaginary part interference. In Ref. [4], we called this the correction factor $C(\equiv 1 + \Delta C)$:

$$C \equiv \frac{\sigma_{\rm mNWA}}{\sigma_{\rm prod} \cdot {\rm Br}} = 1 + \frac{2w}{R} \sin\phi, \tag{9}$$

[2]Of course, the cancellation is not perfect because of the strong $\hat{s}$ dependence of the gluon luminosity.

where $\sigma_{\rm mNWA}$, whose subscript denotes *modified* NWA, is the total signal rate by including the imaginary-part interference effect. In the pure imaginary case ($\cos\phi = 0$) there are three unique shapes of a resonance: a pure dip ($C < 0$), a pure peak ($C > 0$), or a nothingness ($C = 0$). Note that the C factor is measurable by comparing the observed event rate with the simulation result of $\sigma_{\rm prod} \cdot {\rm Br}$.

(ii) *Fine bin.*—In an ideal situation with very small bin size, the $m_{\rm inv}$ dependence of $\sigma_{\rm sig}$ can be measured, which is more crucial in observing the dip-peak structure with nonzero real-part interference. When $\cos\phi \neq 0$, the full resonance shape of $\hat{\sigma}_{\rm sig}(m_{\rm inv})$ is a dip-peak (peak-dip) structure if ${\rm sign}(\cos\phi) = +1(-1)$. In order to quantify the signal rates of the dip and peak, we define the relative height $\hat{h}^+$ and depth $\hat{h}^-$, compared with the height of the BW peak. In addition, the relative widths of the peak and dip are defined as $\hat{w}^\pm$, as illustrated in Fig. 2. For the general case with both real- and imaginary-part interference, we obtain $\hat{h}^\pm$ and $\hat{w}^\pm$ in terms of our key parameters as

$$\hat{h}^\pm = \frac{1}{2}\left[\sqrt{C^2 + \left(\frac{2w\cos\phi}{R}\right)^2} \pm C\right],$$
$$\hat{w}^\pm = \sqrt{\left(\frac{2w\cos\phi}{R}\right)^2 - 1 \pm 2C}. \quad (10)$$

Note that $\hat{w}^-$ is not defined if $(2w\cos\phi/R)^2 < 1 + 2C$ when $C > 0$: this is because we defined $\hat{w}^-$ as the width at the negative half maximum of the BW one. If the dip is shallow such that its depth is smaller than the BW half maximum, we do not calculate $\hat{w}^-$ as considering it as a shallow dip.

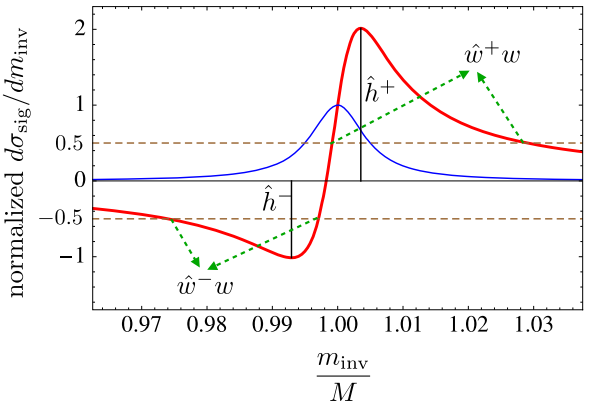

FIG. 2. The definitions of variables characterizing a resonance shape in Eq. (10): the relative height $\hat{h}^+$ and depth $\hat{h}^-$, the relative peak width $\hat{w}^+$, and the relative dip width $\hat{w}^-$ for $w = 0.01$, $R = 0.007$, and $\phi = 0$. We normalized the differential cross section about the invariant mass such that the peak height of the BW resonance without any interference (blue) is a unity.

Two limiting cases ($2w/R \ll 1$ and $2w/R \gg 1$) present a clear understanding of the real part interference effect. When $\sin\phi = 0$, Eq. (10) to leading order becomes

$$\hat{h}^+ \simeq \hat{h}^- \simeq \frac{w}{R}, \quad \hat{w}^+ \simeq \hat{w}^+ \simeq \frac{2w}{R}, \quad \text{if } \frac{2w}{R} \gg 1; \quad (11)$$

$$\hat{h}^+ \simeq 1, \quad \hat{h}^- \simeq 0, \quad \hat{w}^+ \simeq 1, \quad \text{if } \frac{2w}{R} \ll 1. \quad (12)$$

It is clear that the total width is not the key parameter which determines the real part interference, but the ratio w/R is. Even though Γ is very small compared to its mass M, smaller R can make the ratio w/R large: we have a profound dip-peak structure with enhanced height and enhanced width: see Eq. (11). If $w/R \ll 1$, we have a very shallow dip and a BW-like peak as shown in Eq. (12).

On the analogy of the correction factor C, which quantifies the integrated resonance signal rate with the interference, we suggest two new factors, the distribution factors D^+ and D^-, defined by

$$D^\pm = \hat{h}^\pm \hat{w}^\pm. \quad (13)$$

Note that $D^\pm$ is not exactly proportional to the new physics signal rate, since the resonance shape with interference is different from the ordinary BW form. However these simple factors provide a powerful estimate for the dip-peak structure, especially useful when scanning a theoretical parameter space in order to look for the large real-part interference effect. If $D^- = 1$ for example, we can expect that a dip shall appear with almost the same rate with the BW resonance.

III. $\gamma\gamma$ CHANNEL

The diphoton decay channel of a heavy neutral Higgs boson H produced by the gluon-gluon fusion is a two-loop process while the SM continuum background $gg \to \gamma\gamma$ is a one-loop process.[3] The parton level differential cross section of $gg \to \gamma\gamma$ is

[3]We do not consider the subdominant two-loop contribution in continuum background. Its effect on the resonance-continuum interference was shown to be 5% when $M_H < 160$ GeV [5,47].

$$\frac{d\hat{\sigma}(gg\to\gamma\gamma)}{dz}=\frac{1}{32\pi\hat{s}}\frac{\alpha_s^2\alpha_e^2}{2}\sum_{\lambda_1\lambda_2\lambda_3\lambda_4}|\mathcal{M}^{\rm cont}_{\lambda_1\lambda_2\lambda_3\lambda_4}+\mathcal{M}^{H}_{\lambda_1\lambda_2\lambda_3\lambda_4}|^2, \tag{14}$$

where $\mathcal{M}^{\rm cont,H}_{\lambda_1\lambda_2\lambda_3\lambda_4}$ are the normalized helicity amplitudes from the continuum background and H resonance with the helicity of incoming gluons (λ_1,λ_2) and outgoing photons (λ_3,λ_4). The overall factor is due to the loop correction. We refer the explicit expressions of $\mathcal{M}^{\rm cont}$'s to Refs. [21,48]. For the Higgs resonance signal $gg\to H\to\gamma\gamma$, only four helicity amplitudes are nonzero:

$$\begin{aligned}\mathcal{M}^{H}_{++++}&=\mathcal{M}^{H}_{----}=\mathcal{M}^{H}_{++--}=\mathcal{M}^{H}_{--++}\\&=\frac{G_F}{128\pi^2}\frac{\hat{s}^2}{\hat{s}-M_H^2+iM_H\Gamma_H}\sum_q\hat{y}^H_qA^H_{1/2}(\tau_q)\\&\quad\times\left(\sum_q\hat{y}^H_qN_cQ_q^2A^H_{1/2}(\tau_q)\right.\\&\quad\left.+\sum_\ell\hat{y}^H_\ell Q_\ell^2A^H_{1/2}(\tau_\ell)+c_{\beta-\alpha}A^H_1(\tau_W)\right),\end{aligned} \tag{15}$$

where $\tau_p=\hat{s}/(4m_p^2)$, and $\hat{y}^H_{q,\ell}$'s are shown in Eq. (4), and the expressions of $A^H_{1/2,1}(\tau)$ are in Ref. [49].

We first study the relative complex phase ϕ. The complex phase arises through the loop diagrams when the squared of the momentum that passes through an internal cut line is greater than the threshold mass square in the loop. The continuum background $gg\to\gamma\gamma$ is dominated by light quark (u, d, s, c, b) loops whose complex phase arises in $(+-+-)$, $(-++-)$, $(+--+)$, $(-++-)$ helicity amplitudes. But, those helicity amplitudes do not inference with the Higgs resonance amplitudes as can be clearly seen in Eq. (15). Then, only the top quark loop can give a small contribution to the complex phase. The relative phase ϕ is mainly from the Higgs resonance. $gg\to H\to\gamma\gamma$ is dominated by the top quark loop and the W boson loop where the latter is suppressed for small $c_{\beta-\alpha}$. When $M_H<2m_t$ the imaginary part of amplitude arises mostly from the W loop while after $M_H>2m_t$ from the top quark loop. If both $c_{\beta-\alpha}$ and $\hat{y}^H_t$ are positive like the SM Higgs boson, two contributions are destructive.

In Fig. 3, we show ϕ with respect to M_H for several benchmark parameter points of $c_{\beta-\alpha}$ and t_β. We set $c_{\beta-\alpha}=\pm0.4$ for type I and $c_{\beta-\alpha}=\pm0.1$ for type II, which are marginally allowed by the current Higgs precision measurement. In both types, there is a considerable portion of parameter space where the imaginary-part interference is large, i.e., sizable $\sin\phi$.

For type I, we consider four cases of $c_{\beta-\alpha}=\pm0.4$ and $t_\beta=1,10$. The value of ϕ is determined by the behaviors of the real and imaginary parts of the loop functions at the given mass M_H. For example, let us focus on $M_H=200$ GeV where the W loop mainly generates a phase. The case $(c_{\beta-\alpha}=0.4,t_\beta=1)$ has ϕ near zero while the other three cases have large negative values near $-\pi/2$. As shown in Fig. 1, $(c_{\beta-\alpha}=0.4,t_\beta=1)$ leads to negative $\hat{y}_t$ so that the top quark loop and the W loop become constructive: the real part of the total loop function become larger; the phase ϕ is small. For the other three cases, the destructive interference reduces the real parts of the loop function significantly. The untouched imaginary loop function part, which is negative in these cases, yields $\phi\sim-\pi/2$. For other M_H, a similar understanding is possible through the relative strengths and signs of $\hat{y}_{t,b}$ and $c_{\beta-\alpha}$. The abrupt change of amount π in ϕ at $M_H=600$ GeV for $c_{\beta-\alpha}=-0.4$ and $t_\beta=10$ is attributed to the cancellation of two real parts between W and top loops and consequent sign flip.

For type II, the four cases of $c_{\beta-\alpha}=\pm0.1$ and $t_\beta=1,10$ are considered. The small values of $c_{\beta-\alpha}=\pm0.1$ suppress the W loop contribution. The imaginary phase occurs in the loop function $A^H_{1/2}(\tau_t)$ when $M_H>2m_t$. For $M_H<2m_t$, ϕ is close to zero except for the case $(c_{\beta-\alpha}=-0.1,t_\beta=10)$

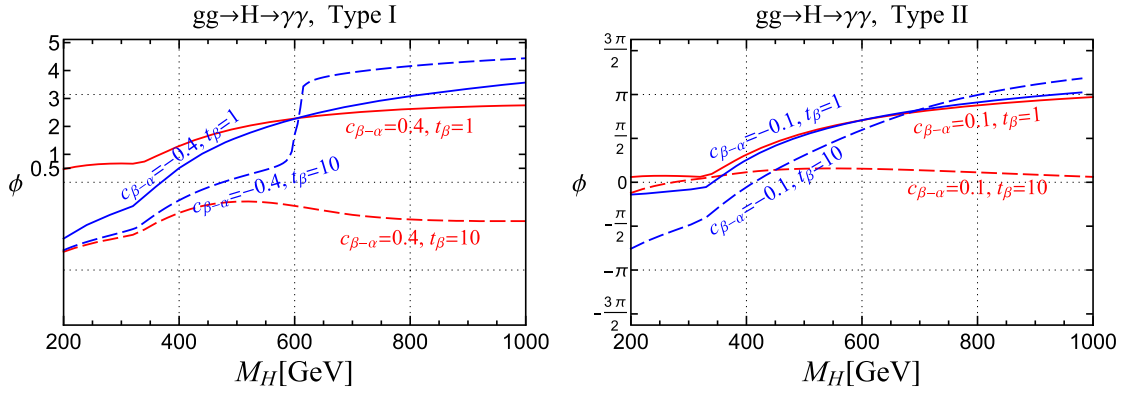

FIG. 3. The resonance-continuum interference phase ϕ of the $gg\to(H\to)\gamma\gamma$ process for various benchmark parameter values of $c_{\beta-\alpha}$ and t_β in the type I (left panel) and type II (right panel) models. The abrupt change at around $M_H\simeq2m_t$ is due to the onset of top-pair threshold.

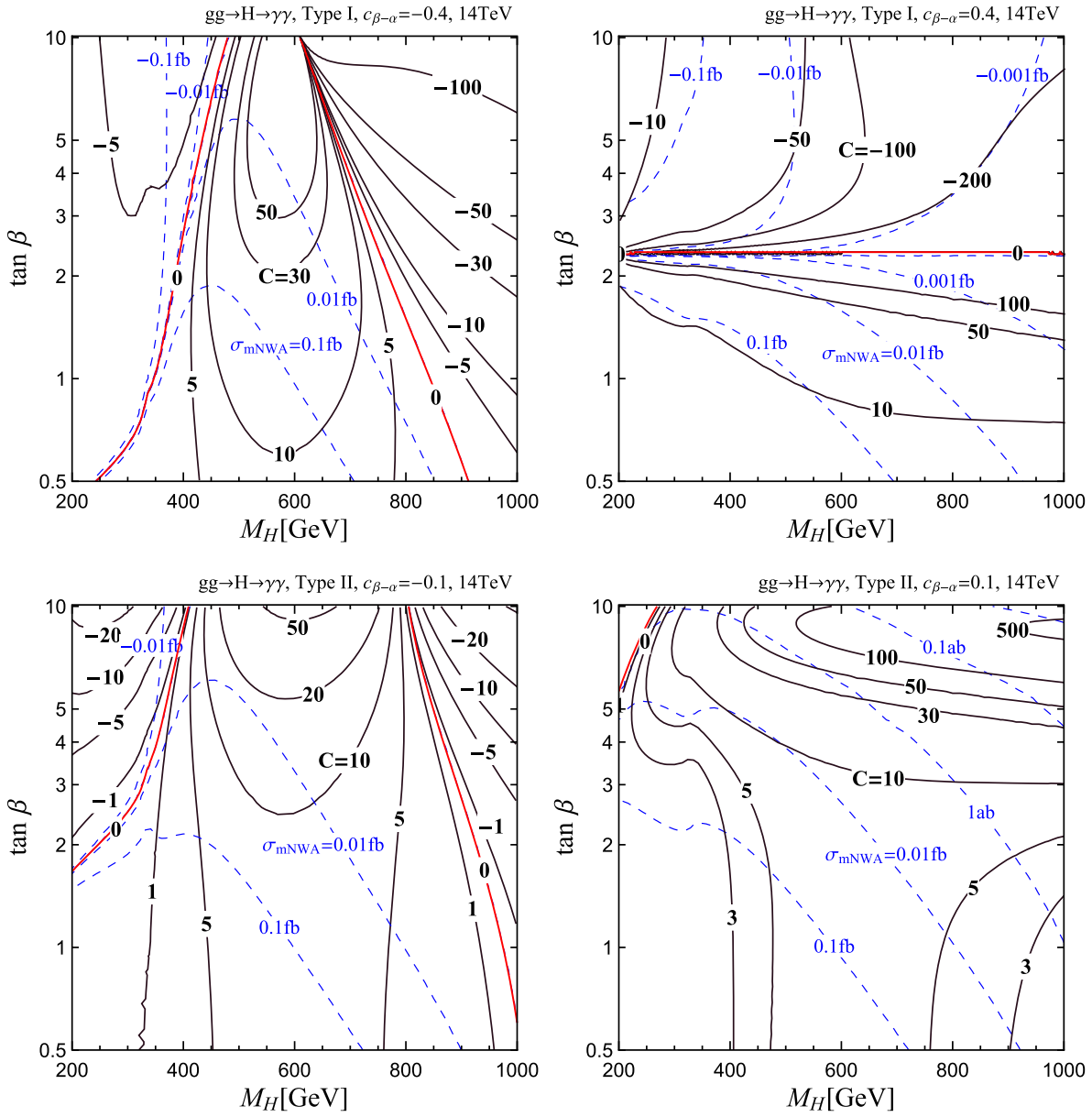

FIG. 4. Contours of the C factor (solid black) and the $\sigma_{\rm mNWA}$ (dashed blue) of the $gg \to H \to \gamma\gamma$ process at the LHC 14 TeV in the $(M_H,\ t_\beta)$ plane. The contour of $C = 0$ is marked with red-solid.

where the sizable b quark contribution with large t_β considerably cancels the whole real part and ϕ has a large negative value. As M_H crosses the $2m_t$ threshold, ϕ continually increases up to π except for the $(c_{\beta-\alpha} = 0.1, t_\beta = 10)$ case. Here the real part of $A^H_{1/2}(\tau_t)$ vanishes when $M_H = 1.1$ TeV so that the one-loop function generates the phase of $\pi/2$. Two factors of $A^H_{1/2}(\tau_t)$ from production and decay processes yield $\phi = \pi$. The exceptional $(c_{\beta-\alpha} = 0.1, t_\beta = 10)$ case is near the top-phobic line. In this case, real parts of the W loop and the bottom quark loop are added up while some cancellation arises for the imaginary part. Therefore, ϕ is very small along the whole M_H region.

Second, we examine w and R in $gg \to \gamma\gamma$, of which the ratio w/R is the crucial factor to determine the interference effects. For simplicity, we assume that H decays into $WW, ZZ, q\bar{q}, \tau\tau, \gamma\gamma$. The possibly important decay channel $H \to hh$ is neglected, which can be achieved by tuning the soft Z_2 symmetry breaking term m^2_{12}. Since this assumption minimizes the total width and thus the interference effects, it shows a good limiting feature of the interference effects in $gg \to \gamma\gamma$. The effect of additional decay channels shall be discussed in Sec. V. Under this assumption, the Γ_H, which generally increases with M_H, depends on $c_{\beta-\alpha}$ and t_β. If $c_{\beta-\alpha} = \pm 0.1$, the parameter w for $M_H \lesssim 1$ TeV is very small to be $\mathcal{O}(10^{-3}) - \mathcal{O}(10^{-2})$ depending on the t_β value

since $H \to WW, ZZ$ is very suppressed. If $c_{\beta-\alpha} = \pm 0.4$ the WW, ZZ decay channels become quite significant so that Γ_H can be 100 GeV until $M_H < 1$ TeV.

The R value, proportional to the ratio of the magnitude of the signal amplitude to that of the background amplitude, is generically small in $gg \to \gamma\gamma$. The background process is at one loop and the H signal is at two loops. The ratio R is roughly one-loop suppressed. In most of the parameter space R is less than 10^{-3}. We have very large interference effects.

Now we quantitatively discuss the interference effects. In Fig. 4, we show the contour plots for the C factor as well as the modified total signal rate $\sigma_{\rm mNWA} = C \times (\sigma \cdot {\rm Br})$ at 14 TeV in (M_H, t_β) plane for $c_{\beta-\alpha} = \pm 0.4$ in type I and $c_{\beta-\alpha} = \pm 0.1$ in type II. For the initial gluon luminosity, we used the CT10NLO PDF set [50]. We also applied next-to-next-to leading order k-factor to the heavy Higgs resonance production part using HIGLU Fortran package [51] and use the leading order decay rate of heavy Higgs in Ref. [52].

The most unexpected result is that the interference effect $|\Delta C|$ can be $\mathcal{O}(100)\%$ even when w is sub-percent level ($c_{\beta-\alpha} = \pm 0.1$ and large t_β). The usually adopted criteria to ignore the interference effect, $w \ll 1$, is not good enough. The characteristics of C values for different type and parameters are as follows. The C contours for $c_{\beta-\alpha} < 0$ show some common features in both type I and type II. They have three sectors divided by two $C = 0$ lines. The left and right parts of these lines have large negative C factors (diplike resonance shapes), while the middle region has positive C factors (peaklike resonance shapes). The two $C = 0$ lines appear near two points $\phi \simeq 0$ and $\phi \simeq \pi$, where ΔC flips its sign (here $2w/R$ is very large). As shown in Fig. 3(b), crossing $\phi = 0, \pi$ happens 2 times for 200 GeV $< M_H <$ 1 TeV, which passes near two $C = 0$ lines. In addition, the magnitude of C increases with increasing t_β. This is because the signal amplitude (or R) is reduced by increasing t_β. On the contrary $\sigma_{\rm mNWA}$ decreases with increasing t_β. In the type II $c_{\beta-\alpha} = 0.1$ case, there is only one $C = 0$ line since ϕ crosses the $\phi = 0$ point once when $t_\beta = 10$: see Fig. 3(b).

For the $c_{\beta-\alpha} > 0$ case of type I, there is one horizontal $C = 0$ line. However, the origin of $C = 0$ here is different from the other three cases. It is very close to the top-phobic (actually fermion-phobic due to the common $\hat{y}^H$'s for all fermions) line as in Fig. 1. This fermion-phobic nature prohibits the gluon fusion production itself. In the vicinity of the $C = 0$ line, very small R is generated, enhancing C extremely. Since the sign of top Yukawa coupling is flipped at this line, so does the sign of C. Another unexpected result is that the large t_β region in type I has compatible signal rate with the small t_β region since $\hat{y}_t^H$ increases again with t_β after crossing the top-phobic line. Our final observation is that $|\Delta C|$ and $\sigma_{\rm mNWA}$ are anticorrelated in general: the region for large $|\Delta C|$ usually has very suppressed signal rate.

IV. ZZ CHANNEL

For the ZZ channel, both the SM background process $gg \to ZZ$ and the Higgs resonance signal $gg \to H \to ZZ$ are one-loop processes. The partonic differential cross section is

$$\frac{d\hat{\sigma}(gg \to ZZ)}{dz} = \frac{1}{32\pi\hat{s}} \frac{\alpha_s^2 \alpha_Z^2 \beta_Z}{256} \sum_{\lambda_1\lambda_2\lambda_3\lambda_4} |\mathcal{T}^{\rm cont}_{\lambda_1\lambda_2\lambda_3\lambda_4} + \mathcal{T}^{H}_{\lambda_1\lambda_2\lambda_3\lambda_4}|^2, \tag{16}$$

where $\alpha_Z = \alpha_e/(\sin^2\theta_W \cos^2\theta_W)$ with weak mixing angle θ_W and $\beta_Z = \sqrt{1-4m_Z^2/\hat{s}}$. $\mathcal{T}^{\rm cont}$ and $\mathcal{T}^H$ are the normalized helicity amplitude for the background and H signal, respectively, of which the expressions are referred to Ref. [8].[4] A big difference between $\mathcal{T}^{\rm cont}(gg \to ZZ)$ and $\mathcal{M}^{\rm cont}(gg \to \gamma\gamma)$ is the presence of the longitudinal mode in the ZZ channel. In particular when both outgoing Z bosons are longitudinal (called the LL mode), the amplitude is proportional to m_q^2. In the ZZ mode, therefore, the top quark contribution becomes important after the $t\bar{t}$ threshold. We found that the LL contribution increases linearly with m_{ZZ}, reaching about 50% at $m_{ZZ} = 700$ GeV.

We first study the complex phase ϕ in the ZZ channel. For the background process, the complex phase from the top quark loop significantly increases with invariant mass m_{ZZ} after the $t\bar{t}$ threshold while the light quark contribution to $\phi_{\rm cont}$ decreases quickly. For $gg \to H \to ZZ$, the top quark loop contribution to $gg \to H$ provides a dominant complex phase unless the b contribution becomes dominant for large t_β in type II. It appears that the behaviors of complex phases of the top loop contributions from $gg \to ZZ$ and $gg \to H \to ZZ$ are quite similar after $M_H > 2m_t$. As a result, the phase $\phi \sim (\phi_{\rm res} - \phi_{\rm cont})$ is close to 0 or π depending on overall sign. This is clearly shown in Fig. 5. One exception is the case $(c_{\beta-\alpha} = 0.1, t_\beta = 10)$ in type II (green-colored line), which corresponds to top-phobic H: ϕ is quite different from 0 or π. Here the bottom quark loop is dominant. We also found that type I shows special behavior: only two curves appear regardless of $c_{\beta-\alpha}$ and t_β. It is because all $\hat{y}^H$'s are the same and thus $\phi_{\rm res}$ is also the same except the overall sign. For example, $c_{\beta-\alpha}\hat{y}^H$ in the case $(c_{\beta-\alpha} = 0.4, t_\beta = 1)$ has the opposite sign of that in the other three cases: see Fig. 1.

Now, we investigate C factor and $\sigma_{\rm mNWA}$. The basic setup is similar to the $\gamma\gamma$ channel. The w parameter is small in general. The R is roughly $\mathcal{O}(0.01)$, mostly larger than w,

[4] $\mathcal{T}_{\lambda_1\lambda_2\lambda_3\lambda_4}$ are corresponding to $\mathcal{M}_{\lambda_1\lambda_2\lambda_3\lambda_4}$ in Ref. [8]. There is an obvious typo in Eq. (3.14) of Ref. [8] since the mass dimensions of the first two terms in curly brackets of the right-hand side are incorrect. From the independent calculation, we find that it should be $(1+\beta)\{4s(t-u)Y/(s_4 u_1 t_1) + 4Y/s_4(\cdots) + \cdots\}$ where the ellipses represent the same form of the equation.

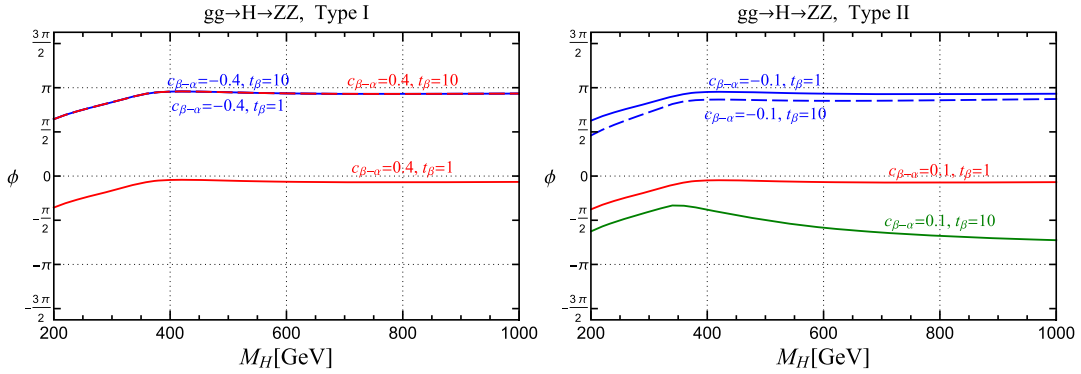

FIG. 5. The resonance-continuum interference phase ϕ of the $gg \to (H \to)ZZ$ process for various benchmark parameter values of $c_{\beta-\alpha}$ and t_β in the type I (left panel) and type II (right panel) models. The abrupt change at around $M_H \simeq 2m_t$ is due to the onset of top-pair threshold. The top-phobic case is shown as the green solid line.

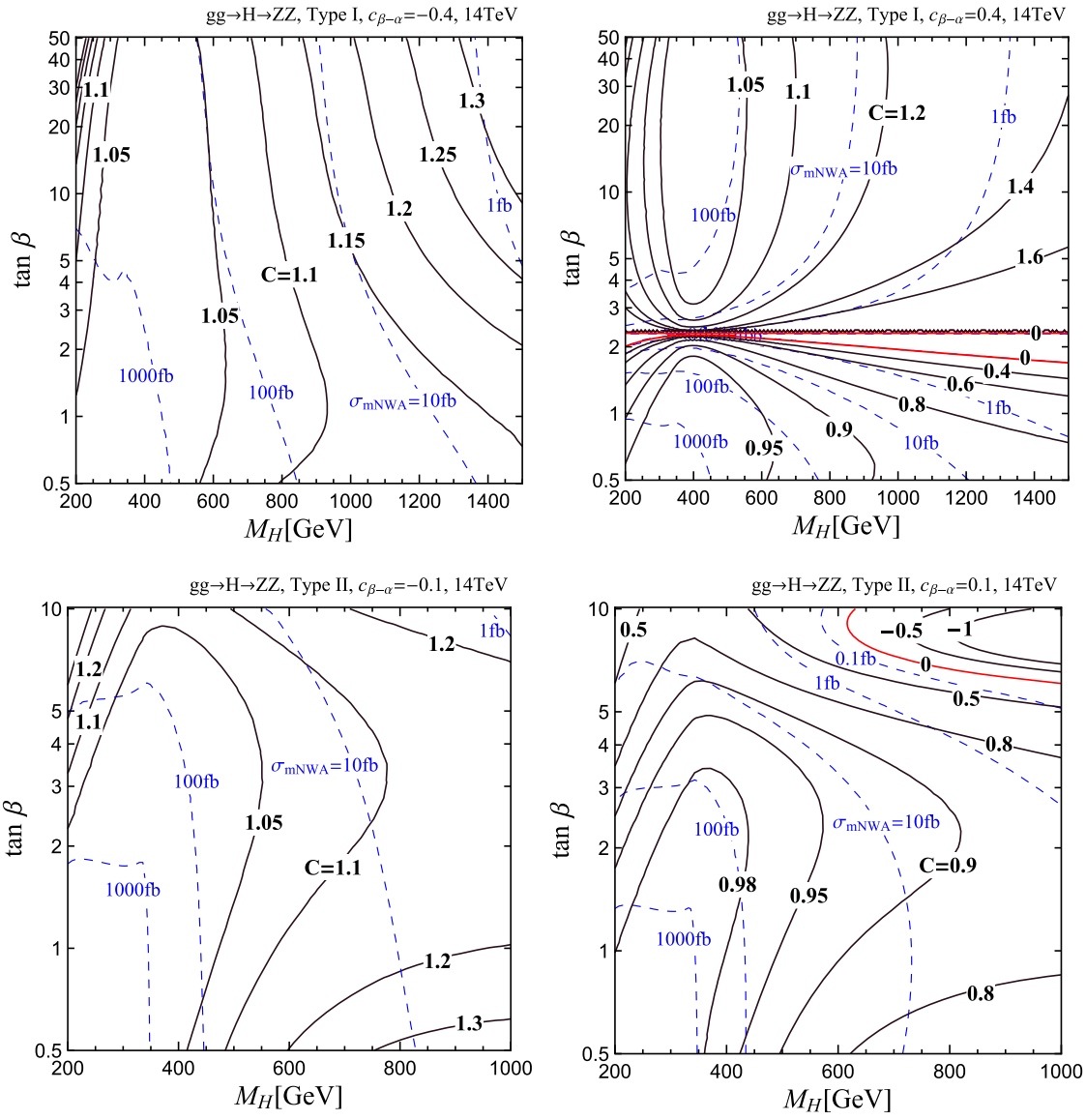

FIG. 6. Contours of the C factor (solid black) and the $\sigma_{\rm mNWA}$ (dashed blue) of the $gg \to H \to ZZ$ process at the LHC 14 TeV in the (M_H, t_β) plane. The contour of $C = 0$ is marked with red solid.

since both the SM background process and the Higgs resonance signal are one-loop processes. The interference effect would be generically small in the ZZ channel for small w. Moreover, the $c_{\beta-\alpha}$ value does not affect the ratio w/R much since larger $c_{\beta-\alpha}$ increases both R and w.

In Fig. 6, we show the contours of the C factor and σ_{mNWA} in the (M_H, t_β) plane for $c_{\beta-\alpha} = \pm 0.4$ for type I and $c_{\beta-\alpha} = \pm 0.1$ for type II. The first important result is that the interference effect is not negligible even when w is very small, though not dramatic as in the $\gamma\gamma$ channel. For example, the case of $M_H = 300$ GeV, $c_{\beta-\alpha} = 0.1$, and $t_\beta = 10$ in type II, where $\Gamma_H/M_H = 0.2\%$, has $\Delta C \simeq -30\%$. The second result is that for the given t_β, $|\Delta C|$ decreases with M_H but increases again after the $t\bar{t}$ threshold. Before the $t\bar{t}$ threshold R increases much faster than w. After the $t\bar{t}$ threshold, w increases more sharply as the $t\bar{t}$ decay channel is opened.

The negative $c_{\beta-\alpha}$ case has very smooth and moderate variation of C. We have maximally 30% of ΔC for large t_β and light $M_H \simeq 200$ GeV or very heavy M_H. The positive $c_{\beta-\alpha}$ case allows the top-phobic lines and thus the $C = 0$ line. Similar to the $\gamma\gamma$ channel, the $c_{\beta-\alpha} = 0.4$ case in type I has two $C = 0$ lines which are narrowly split near the top-phobic line. Near this top-phobic line $|\Delta C|$ is much enhanced since R is very suppressed. Note that the large signal rate region, with small M_H and some deviation from

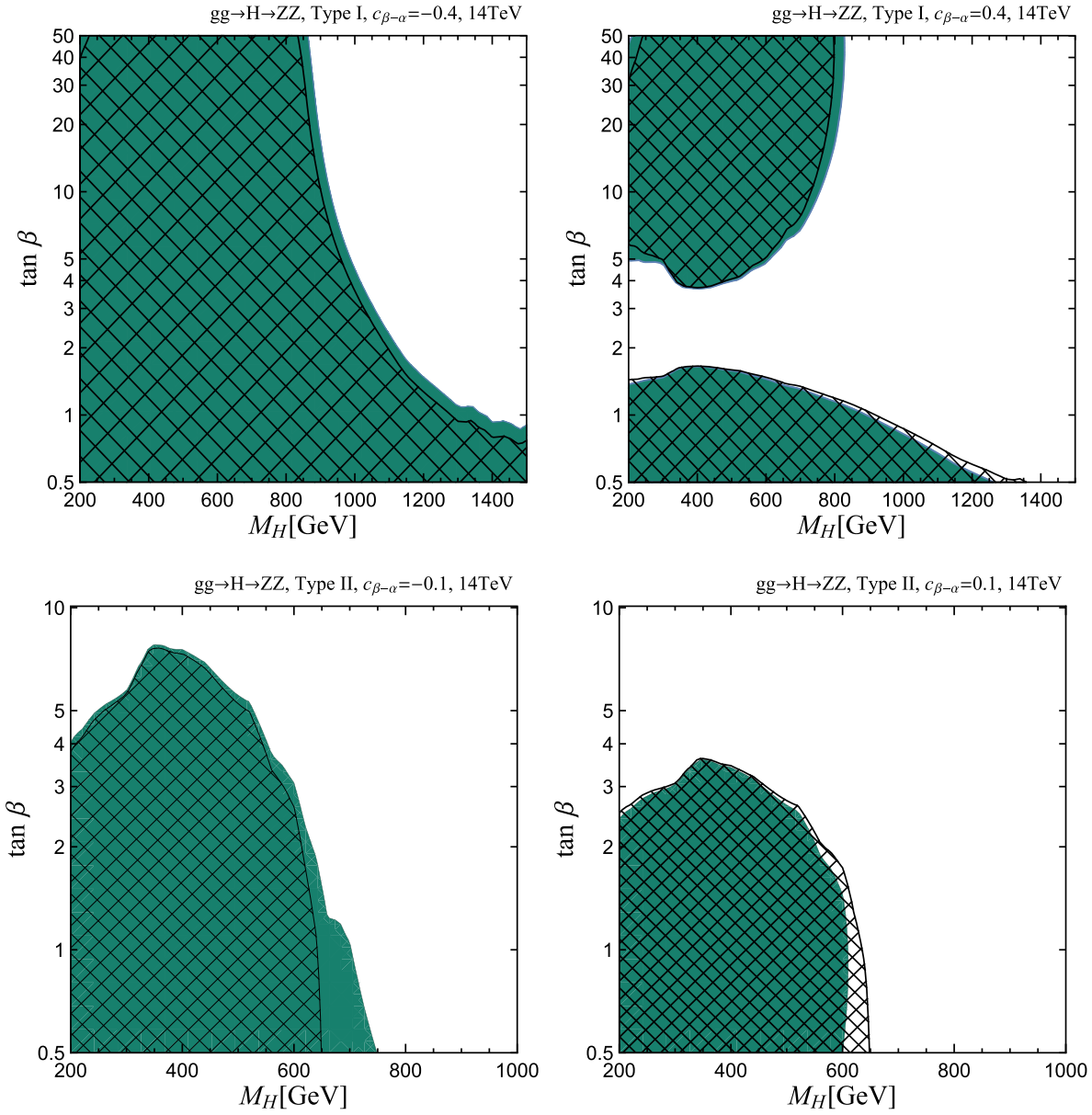

FIG. 7. Expected exclusion regions from ZZ resonance searches at the 14 TeV LHC with 300 fb^{-1}, projected from the LHC 8 TeV results. The green regions include interference effects and the hatched regions are without interferences. We used the mNWA to obtain these results assuming that a resonance shape is approximately a BW peak.

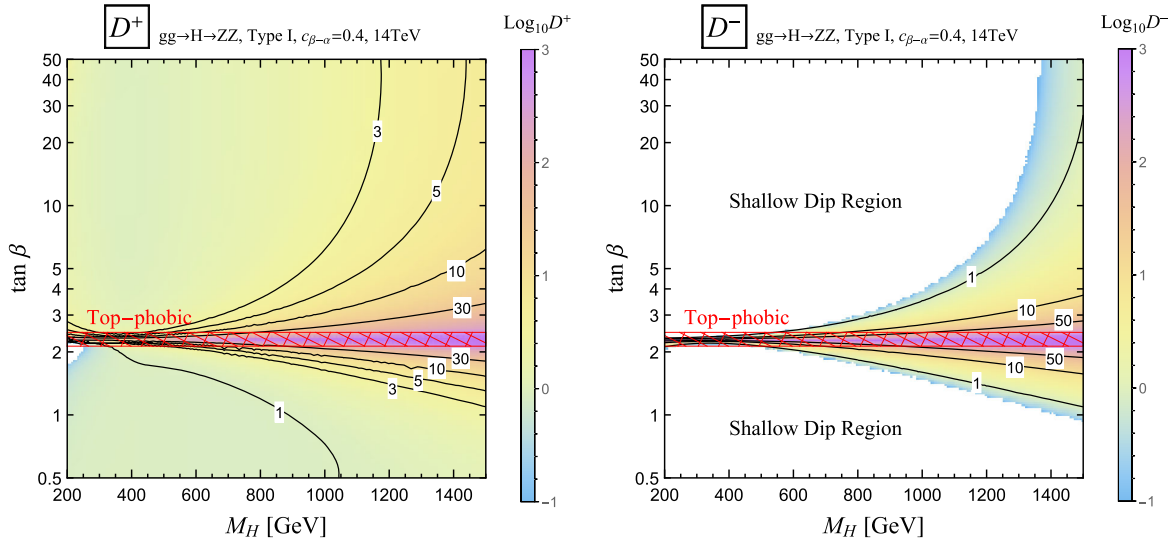

FIG. 8. Contours of D^+ (left) and D^- (right) in the $gg \to H \to ZZ$ process at the 14 TeV LHC for $c_{\beta-\alpha} = 0.4$ in type I. $D^\pm$ are defined in Eq. (13). The red hatched region is around the top-phobic line such that $|\hat{y}_t^H| < 0.03$.

the top-phobic line, has small ΔC. The $c_{\beta-\alpha} = 0.1$ case in type II allows one $C = 0$ line, below which ΔC is negative. For $M_H = 200$ GeV and $t_\beta \simeq 5$–10, the reduction is about 50%.

We now investigate the interference effect on the future experimental sensitivity for the heavy Higgs boson via the ZZ channel. We use the current experimental results on the heavy neutral Higgs search in the ZZ decay channel with 20.3 fb^{-1} data at 8 TeV from ATLAS collaboration [30]. The nonobservation of any significant excess above the background is interpreted as an upper bound on $\sigma(gg \to H \to ZZ)$ as a function of Higgs mass M_H. We project the results for 14 TeV LHC with 300 fb^{-1} data by assuming that the statistical error is dominant [53,54].

In Fig. 7, we show the 14 TeV LHC projections of the exclusion plots in the (M_H, t_β) plane for 300 fb^{-1} data. We set $c_{\beta-\alpha} = \pm 0.4$ in type I and $c_{\beta-\alpha} = \pm 0.1$ in type II. The hatched exclusion region is obtained by using naive NWA (without interference effect) while the green-colored exclusion region by mNWA (with interference effect). For type I, we extend the exclusion region up to 1.5 TeV by applying a simple extrapolation. For $c_{\beta-\alpha} = -0.4$ the exclusion region covers the entire t_β region up to $M_H = 830$ GeV and the interference effect enlarges the exclusion region by 20–30 GeV, i.e., constructive interference. For $c_{\beta-\alpha} = 0.4$, there are two separate exclusion regions divided by the top-phobic line. The upper (lower) region shows constructive (destructive) interference effect. Because of sizable top-quark Yukawa coupling above the top-phobic line, the large t_β region ($5 < t_\beta < 50$) up to $M_H = 800$ GeV also can be reached by LHC run II data. As for type II, for $c_{\beta-\alpha} = 0.1$ ($c_{\beta-\alpha} = -0.1$) the interference effect is constructive (destructive).

Finally, we demonstrate the real-part interference effect by showing the contours of D^+ and D^- in the (M_H, t_β) plane: see Fig. 8. We take the case for $c_{\beta-\alpha} = 0.4$ in type I at 14 TeV LHC, which brings about large real-part interference effects.[5] The behaviors of $D^\pm$ are quite similar to C: $D^\pm$ is large near the top-phobic line where R is small. For D^-, the uncolored region indicates that the dip is shallower than the half maximum of the BW peak. Even in this shallow dip region, D^+ can be up to 5, which is attributed to highly asymmetric m_{ZZ} distribution near $\hat{s} = M^2$. Note that the corresponding $|\Delta C|$ factor is less than ~40%. The real-part interference can be more important, which is observable if the detector resolution is good enough to separate the peak from the dip. Once the dip is deep enough (colored region), both $D^\pm$ are larger than 1: a clear dip-peak ($c_\phi > 0$) or peak-dip ($c_\phi < 0$) shape is expected. The line-shape analysis can serve as another important probe for the heavy Higgs signal.

V. ROLE OF TOTAL DECAY WIDTH

So far, we have assumed that the heavy H decays into the SM fermions or gauge bosons just as the SM Higgs boson. However, there exist additional decay channels like $H \to hh, ZA, W^\pm H^\mp$ in the 2HDM. As a benchmark scenario in type II, we consider

$$c_{\beta-\alpha} = -0.1, \quad t_\beta = 1.8, \quad m_{12} = 240\,\text{GeV},$$
$$M_H = 550\,\text{GeV}, \quad M_A = 350\,\text{GeV}, \quad M_{H^+} = 350\,\text{GeV}, \tag{17}$$

[5] In the other three cases, the real-part interference is mostly minor.

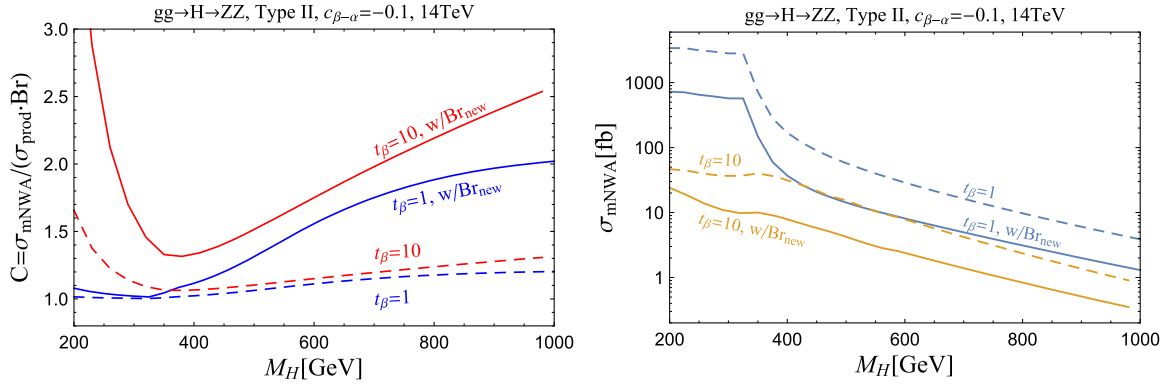

FIG. 9. Plots of C factor and $\sigma_{\rm mNWA}$ with respect to M_H for $gg \to H \to ZZ$ with some parameter choices. Solid lines include the new decay channel with $\mathrm{Br}_{\rm new} = 0.8$ while dashed lines do not.

which satisfies the constrains from $b \to s\gamma$ [55,56], $\Delta\rho$ [57,58] as well as the stability and perturbativity [37,59]. Then additional decay channels have sizable branching ratio: $\mathrm{Br}(H \to hh) = 0.004$, $\mathrm{Br}(H \to ZA) = 0.25$, and $\mathrm{Br}(H \to W^{\pm}H^{\mp}) = 0.54$. Or 2HDM can be extended to include a dark matter candidate χ, allowing a new decay channel of $H \to \chi\chi$. The resulting increase in w shall affect the interference effect: ΔC is enhanced while $\mathrm{Br}(H \to ZZ)$ and thus $\sigma_{\rm mNWA}$ are reduced. Figure 9 shows the plots of C and $\sigma_{\rm mNWA}$ with $\mathrm{Br}_{\rm new} = 0.8$ and some specific parameter choices in the ZZ channel. The magnitude of $|\Delta C|$ is significantly enhanced by a factor of about 5. As discussed before, $\sigma_{\rm mNWA}$ is much reduced.

Finally, we illustrate how dramatically the resonance shape can be altered by changing the total width. Figure 10 shows the m_{ZZ} distribution for a benchmark point of $M_H = 600$ GeV, $c_{\beta-\alpha} = 0.1$ and $t_\beta = 8$ in type II, which yields $R = 0.0063$, $\phi = -74°$, and $\sigma \cdot \mathrm{Br} \simeq 0.4$ fb. If H decays into the SM fermions and gauge bosons only, the total decay width is small ($w = 0.27\%$) and $\Delta C = -83\%$. The resonance shape is a suppressed dip-peak structure, as denoted by the yellow solid line. If we further allow a sizable branching ratio of a new decay channel like $\mathrm{Br}_{\rm new} = 0.8$, the m_{ZZ} distribution shape changes into a new form, a pure dip (the red solid line). Three m_{ZZ} distribution lines clearly show that measuring the invariant mass distribution would serve as a multidimensional projection to extract the information of w, R and ϕ. This is to be compared with measuring the total signal rate only, just a single dimensional projection.

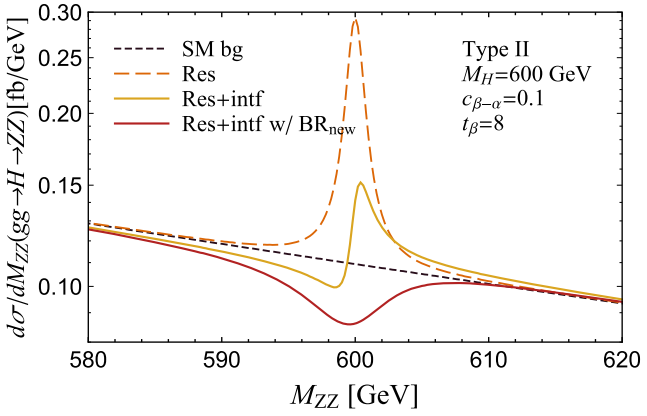

FIG. 10. Example ZZ invariant mass distribution of $gg \to H \to ZZ$ for the given parameter choice. We show several results for comparison: the full result with interferences accounted for (yellow solid), the pure BW result without interferences (orange dashed), the full result with additional decay modes $\mathrm{Br}_{\rm new} = 0.8$ (red solid), and the continuum background $gg \to ZZ$ alone (black dashed).

VI. CONCLUSIONS

We have studied the resonance-continuum interference effects of the heavy neutral Higgs boson H of the nearly aligned type I and II 2HDM in the $\gamma\gamma$ and ZZ channels. Even for the H with a sub-percent width-to-mass ratio, the size and pattern of the interference effects can vary with underlying parameters and can be observably large.

For the parameter space where the ZZ resonance search at the LHC with $\sqrt{s} = 14$ TeV is sensitive (particularly for small $t_\beta \lesssim 1$), the interference effects mildly modify the ZZ signal rate by $\mathcal{O}(10)\%$ and change the exclusion reach on the M_H by $\mathcal{O}(10)$ GeV. For example, the benchmark parameter $M_H = 300$ GeV, $c_{\beta-\alpha} = 0.1$, and $t_\beta = 10$ (yielding $\Gamma_H/M_H = 0.2\%$) modifies the ZZ signal rate by -30% from the interference. In this parameter space, we approximately treated the resonance shape as a BW peak and used the mNWA to estimate a new exclusion reach. In other words, we could use the C-factor to approximately quantify the interference effects (hence, on the signal rate).

In other parameter space where the ZZ signal rate is substantially smaller (such as near the top-phobic line), although it is unreachable for the LHC run at 14 TeV, a resonance shape can be much more dramatically changed. Also for the $\gamma\gamma$ channel, signal rates are smaller and the LHC 14 TeV reach is absent in all parameter space, but the signal rates can be typically modified by $\mathcal{O}(100)\%$ due to

interference effects. For the same parameter choice as in the previous paragraph, the $\gamma\gamma$ signal rate is modified by 400%. In these cases, one shall carry out a more careful collider study of resonance searches including the interference effects. Rather than doing this in this paper, we suggested a few variables that can characterize a general resonance shape defined in Eqs. (10)–(13) and in Fig. 2. It will be worthwhile carrying out a dedicated future collider study.

The interference effects also grow with the resonance width. To illustrate this, we also considered a case with extra nonstandard decay modes of the heavy Higgs boson. The increased width and correspondingly reduced signal could induce more significant interference effects in both channels. For example, with 80% new branching ratio, we find that the ZZ signal rate can be enhanced by a factor 2–3, but a more careful collider study including the modification of a resonance shape will be needed in this case.

From varying sizes of the interference with different signal rates, we verify a general result that we have discussed in Ref. [4]; the smaller the signal rate, the bigger the relative interference. The resonance-to-continuum ratio, approximately measured by R in Eq. (7), is another factor; the smaller the ratio, the bigger the relative interference. This is why the $\gamma\gamma$ channel experiences a bigger relative interference than the ZZ channel does. Looking forward, a 100 TeV pp collider and high-luminosity LHC data that can probe the parameter space with smaller signal rates will generically experience bigger interference effects.

ACKNOWLEDGMENTS

The work of J. S. is supported by NRF-2013R1A1A2061331. The work of Y. W. Y. is supported by NRF-2012R1A2A1A01006053. The work of S. J. is supported by the U.S. Department of Energy under Contract No. DE-AC02-76SF00515. We thank Convergence Computing team of National Institute for Mathematical Sciences for valuable comments in extracting data from experimental papers, and KIAS Center for Advanced Computation for providing computing resources.

[1] G. Aad *et al.* (ATLAS Collaboration), Observation of a new particle in the search for the Standard Model Higgs boson with the ATLAS detector at the LHC, Phys. Lett. B **716**, 1 (2012); S. Chatrchyan *et al.* (CMS Collaboration), Observation of a new boson at a mass of 125 GeV with the CMS experiment at the LHC, Phys. Lett. B **716**, 30 (2012).

[2] K. J. F. Gaemers and F. Hoogeveen, Higgs production and decay into heavy flavors with the gluon fusion mechanism, Phys. Lett. **146B**, 347 (1984).

[3] D. Dicus, A. Stange, and S. Willenbrock, Higgs decay to top quarks at hadron colliders, Phys. Lett. B **333**, 126 (1994).

[4] S. Jung, J. Song, and Y. W. Yoon, Dip or nothingness of a Higgs resonance from the interference with a complex phase, Phys. Rev. D **92**, 055009 (2015).

[5] L. J. Dixon and M. S. Siu, Resonance Continuum Interference in the Diphoton Higgs Signal at the LHC, Phys. Rev. Lett. **90**, 252001 (2003).

[6] S. P. Martin, Shift in the LHC Higgs diphoton mass peak from interference with background, Phys. Rev. D **86**, 073016 (2012).

[7] L. J. Dixon and Y. Li, Bounding the Higgs Boson Width Through Interferometry, Phys. Rev. Lett. **111**, 111802 (2013).

[8] E. W. N. Glover and J. J. van der Bij, Z boson pair production via gluon fusion, Nucl. Phys. **B321**, 561 (1989).

[9] D. A. Morris, T. N. Truong, and D. Zappala, Higgs boson interference in gamma gamma $\to W + W-$, Phys. Lett. B **323**, 421 (1994).

[10] P. Niezurawski, A. F. Zarnecki, and M. Krawczyk, Study of the Higgs boson decays into $W + W$- and ZZ at the photon collider, J. High Energy Phys. 11 (2002) 034.

[11] J. M. Campbell, R. K. Ellis, and C. Williams, Gluon-gluon contributions to $W + W$-production and Higgs interference effects, J. High Energy Phys. 10 (2011) 005.

[12] N. Kauer and G. Passarino, Inadequacy of zero-width approximation for a light Higgs boson signal, J. High Energy Phys. 08 (2012) 116.

[13] N. Kauer, Interference effects for $H\to WW/ZZ\to \ell\bar{\nu}_\ell\bar{\ell}\nu_\ell$ searches in gluon fusion at the LHC, J. High Energy Phys. 12 (2013) 082.

[14] N. Kauer and C. O'Brien, Heavy Higgs signal-background interference in $gg \to VV$ in the Standard Model plus real singlet, Eur. Phys. J. C **75**, 374 (2015).

[15] C. Englert, I. Low, and M. Spannowsky, On-shell interference effects in Higgs boson final states, Phys. Rev. D **91**, 074029 (2015).

[16] N. Kauer, C. O'Brien, and E. Vryonidou, Interference effects for $H \to WW \to lvqq$ and $H \to ZZ \to llqq$ searches in gluon fusion at the LHC, J. High Energy Phys. 10 (2015) 074.

[17] M. Bonvini, F. Caola, S. Forte, K. Melnikov, and G. Ridolfi, Signal-background interference effects for $gg \to H \to W^+W^-$ beyond leading order, Phys. Rev. D **88**, 034032 (2013).

[18] E. Asakawa, J. i. Kamoshita, A. Sugamoto, and I. Watanabe, Production of scalar Higgs and pseudoscalar Higgs in multi-Higgs doublet models at gamma gamma colliders, Eur. Phys. J. C **14**, 335 (2000).

[19] L. J. Dixon and Y. Sofianatos, Resonance-continuum interference in light Higgs boson production at a photon collider, Phys. Rev. D **79**, 033002 (2009).

[20] J. L. Basdevant, E. L. Berger, D. Dicus, C. Kao, and S. Willenbrock, Final state interaction of longitudinal vector bosons, Phys. Lett. B **313**, 402 (1993).

[21] D. A. Dicus and S. S. D. Willenbrock, Photon pair production and the intermediate mass Higgs boson, Phys. Rev. D **37**, 1801 (1988).

[22] W. Bernreuther, A. Brandenburg, and M. Flesch, Effects of Higgs sector *CP* violation in top quark pair production at the LHC, arXiv:hep-ph/9812387.

[23] J. R. Ellis, J. S. Lee, and A. Pilaftsis, Resonant *CP* violation in MSSM Higgs production and decay at gamma gamma colliders, Nucl. Phys. **B718**, 247 (2005).

[24] M. Farina, Y. Grossman, and D. J. Robinson, Probing *CP* violation in $h \to Z\gamma$ with background interference, Phys. Rev. D **92**, 073007 (2015).

[25] L. Bian, D. Liu, J. Shu, and Y. Zhang, Interference effect on resonance searches and the diboson excess, arXiv:1509.02787.

[26] M. Beneke, A. P. Chapovsky, A. Signer, and G. Zanderighi, Effective Theory Approach to Unstable Particle Production, Phys. Rev. Lett. **93**, 011602 (2004).

[27] G. Aad *et al.* (ATLAS Collaboration), Search for Scalar Diphoton Resonances in the Mass Range 65–600 GeV with the ATLAS Detector in pp Collision Data at $\sqrt{s} = 8$ TeV, Phys. Rev. Lett. **113**, 171801 (2014).

[28] (CMS Collaboration), Search for a Higgs-like resonance in the diphoton mass spectra above 150 GeV with 8 TeV data, Report No. CMS-PAS-HIG-14-006.

[29] S. Chatrchyan *et al.* (CMS Collaboration), Measurement of the properties of a Higgs boson in the four-lepton final state, Phys. Rev. D **89**, 092007 (2014).

[30] G. Aad *et al.* (ATLAS Collaboration), Search for an additional, heavy Higgs boson in the $H \to ZZ$ decay channel at $\sqrt{s} = 8$ TeV in pp collision data with the ATLAS detector, Eur. Phys. J. C **76**, 45 (2016).

[31] N. Craig, F. D'Eramo, P. Draper, S. Thomas, and H. Zhang, The hunt for the rest of the Higgs bosons, J. High Energy Phys. 06 (2015) 137.

[32] W. Bernreuther, M. Flesch, and P. Haberl, Signatures of Higgs bosons in the top quark decay channel at hadron colliders, Phys. Rev. D **58**, 114031 (1998); R. Frederix and F. Maltoni, Top pair invariant mass distribution: A window on new physics, J. High Energy Phys. 01 (2009) 047; R. Barcelo and M. Masip, Extra Higgs bosons in $t\bar{t}$ production at the LHC, Phys. Rev. D **81**, 075019 (2010); S. Moretti and D. A. Ross, On the top-antitop invariant mass spectrum at the LHC from a Higgs boson signal perspective, Phys. Lett. B **712**, 245 (2012).

[33] ATLAS Collaboration, A search for $\mathbf{t\bar{t}}$ resonances using lepton plus jets events in proton-proton collisions at $\sqrt{s} =$ 8 TeV with the ATLAS detector, Report No. ATLAS-CONF-2015-009.

[34] S. Chatrchyan *et al.* (CMS Collaboration), Searches for New Physics using the $t\bar{t}$ Invariant Mass Distribution in pp Collisions at $\sqrt{s} = 8$ TeV, Phys. Rev. Lett. **111**, 211804 (2013); **112**, 119903 (2014).

[35] F. Caola and K. Melnikov, Constraining the Higgs boson width with ZZ production at the LHC, Phys. Rev. D **88**, 054024 (2013).

[36] V. Khachatryan *et al.* (CMS Collaboration), Constraints on the Higgs boson width from off-shell production and decay to Z-boson pairs, Phys. Lett. B **736**, 64 (2014).

[37] G. C. Branco, P. M. Ferreira, L. Lavoura, M. N. Rebelo, M. Sher, and J. P. Silva, Theory and phenomenology of two-Higgs-doublet models, Phys. Rep. **516**, 1 (2012).

[38] G. Belanger, B. Dumont, U. Ellwanger, J. F. Gunion, and S. Kraml, Global fit to Higgs signal strengths and couplings and implications for extended Higgs sectors, Phys. Rev. D **88**, 075008 (2013); K. Cheung, J. S. Lee, and P. Y. Tseng, Higgs precision (Higgcision) era begins, J. High Energy Phys. 05 (2013) 134; C. W. Chiang and K. Yagyu, Implications of Higgs boson search data on the two-Higgs doublet models with a softly broken Z_2 symmetry, J. High Energy Phys. 07 (2013) 160; B. Grinstein and P. Uttayarat, Carving out parameter space in type-II two Higgs doublets model, J. High Energy Phys. 06 (2013) 094; 09 (2013) 110 (E); O. Eberhardt, U. Nierste, and M. Wiebusch, Status of the two-Higgs-doublet model of type II, J. High Energy Phys. 07 (2013) 118; A. Celis, V. Ilisie, and A. Pich, LHC constraints on two-Higgs doublet models, J. High Energy Phys. 07 (2013) 053; S. Chang, S. K. Kang, J. P. Lee, K. Y. Lee, S. C. Park, and J. Song, Comprehensive study of two Higgs doublet model in light of the new boson with mass around 125 GeV, J. High Energy Phys. 05 (2013) 075; Two Higgs doublet models for the LHC Higgs boson data at $\sqrt{s} = 7$ and 8 TeV, J. High Energy Phys. 09 (2014) 101.

[39] N. Craig, J. Galloway, and S. Thomas, Searching for signs of the second Higgs doublet, arXiv:1305.2424; A. Celis, V. Ilisie, and A. Pich, Towards a general analysis of LHC data within two-Higgs-doublet models, J. High Energy Phys. 12 (2013) 095; L. Wang and X. F. Han, Status of the aligned two-Higgs-doublet model confronted with the Higgs data, J. High Energy Phys. 04 (2014) 128; P. S. B. Dev and A. Pilaftsis, Maximally symmetric two Higgs doublet model with natural standard model alignment, J. High Energy Phys. 12 (2014) 024.

[40] L. Wang and X.-F. Han, Study of the heavy CP-even Higgs with mass 125 GeV in two-Higgs-doublet models at the LHC and ILC, J. High Energy Phys. 11 (2014) 085.

[41] S. Kanemura, H. Yokoya, and Y. J. Zheng, Complementarity in direct searches for additional Higgs bosons at the LHC and the International Linear Collider, Nucl. Phys. **B886**, 524 (2014).

[42] J. Bernon, J. F. Gunion, Y. Jiang, and S. Kraml, Light Higgs bosons in two-Higgs-doublet models, Phys. Rev. D **91**, 075019 (2015).

[43] B. Coleppa, F. Kling, and S. Su, Constraining type II 2HDM in light of LHC Higgs searches, J. High Energy Phys. 01 (2014) 161.

[44] S. de Visscher, J. M. Gerard, M. Herquet, V. Lemaitre, and F. Maltoni, Unconventional phenomenology of a minimal two-Higgs-doublet model, J. High Energy Phys. 08 (2009) 042.

[45] S. Chang, S. K. Kang, J. P. Lee, and J. Song, Higgs potential and hidden light Higgs scenario in two Higgs doublet models, Phys. Rev. D **92**, 075023 (2015).

[46] P. M. Ferreira, R. Guedes, M. O. P. Sampaio, and R. Santos, Wrong sign and symmetric limits and nondecoupling in 2HDMs, J. High Energy Phys. 12 (2014) 067.

[47] Z. Bern, A. De Freitas, and L. J. Dixon, Two-loop amplitudes for gluon fusion into two photons, J. High Energy Phys. 09 (2001) 037.

[48] V. Costantini, B. De Tollis, and G. Pistoni, Nonlinear effects in quantum electrodynamics, Nuovo Cim. **A2**, 733 (1971).

[49] A. Djouadi, The anatomy of electroweak symmetry breaking. II. The Higgs bosons in the minimal supersymmetric model, Phys. Rep. **459**, 1 (2008).

[50] H. L. Lai, M. Guzzi, J. Huston, Z. Li, P. M. Nadolsky, J. Pumplin, and C.-P. Yuan, New parton distributions for collider physics, Phys. Rev. D **82**, 074024 (2010).

[51] M. Spira, HIGLU: A program for the calculation of the total Higgs production cross section at hadron colliders via gluon fusion including QCD corrections, arXiv:hep-ph/9510347.

[52] J. Song and Y. W. Yoon, Gigantic diphoton rate of heavy Higgs bosons in the aligned two Higgs doublet models with small tan, Phys. Rev. D **91**, 113012 (2015).

[53] S. Jung and J. D. Wells, Gaugino physics of split supersymmetry spectra at the LHC and future proton colliders, Phys. Rev. D **89**, 075004 (2014).

[54] A. Djouadi, L. Maiani, A. Polosa, J. Quevillon, and V. Riquer, Fully covering the MSSM Higgs sector at the LHC, J. High Energy Phys. 06 (2015) 168.

[55] F. Mahmoudi and O. Stal, Flavor constraints on the two-Higgs-doublet model with general Yukawa couplings, Phys. Rev. D **81**, 035016 (2010).

[56] T. Hermann, M. Misiak, and M. Steinhauser, $\bar{B} \to X_s\gamma$ in the two Higgs doublet model up to next-to-next-to-leading order in QCD, J. High Energy Phys. 11 (2012) 036.

[57] J. Gunion *et al.*, *The Higgs Hunter's Guide* (Addison-Wesley, New York, 1990).

[58] P. H. Chankowski, M. Krawczyk, and J. Zochowski, Implications of the precision data for very light Higgs boson scenario in 2HDM(II), Eur. Phys. J. C **11**, 661 (1999).

[59] S. Kanemura, Y. Okada, E. Senaha, and C.-P. Yuan, Higgs coupling constants as a probe of new physics, Phys. Rev. D **70**, 115002 (2004).